Scattering of electromagnetic waves from a cone with conformal mapping: Application to scanning near-field optical microscope

S. T. Chui,[1] Xinzhong Chen,[2] Mengkun Liu,[2] Zhifang Lin,[3] and Jian Zi[3]

[1]*Bartol Research Institute and Department of Physics and Astronomy, University of Delaware, Newark, Delaware, 19716, USA*
[2]*Department of Physics and Astronomy, Stony University, Stony Brook, New York, 11790, USA*
[3]*Department of Physics, Fudan University, Shanghai, 200433, China*

We study the response of a conical metallic surface to an external electromagnetic (em) field by representing the fields in basis functions containing the integrable singularity at the tip of the cone. A fast analytical solution is obtained by the conformal mapping between the cone and a round disk. We apply our calculation to the scattering-type scanning near-field optical microscope (s-SNOM) and successfully quantify the elastic light scattering from a vibrating metallic tip over a uniform sample. We find that the field-induced charge distribution consists of localized terms at the tip and the base and an extended bulk term along the body of the cone far away from the tip. In recent s-SNOM experiments at the visible and infrared range (600 nm to 1 μm) the fundamental of the demodulated near-field signal is found to be much larger than the higher harmonics whereas at THz range (100 μm to 3 mm) the fundamental becomes comparable to the higher harmonics. We find that the localized tip charge dominates the contribution to the higher harmonics and becomes larger for the THz experiments, thus providing an intuitive understanding of the origin of the near-field signals. We demonstrate the application of our method by extracting a two-dimensional effective dielectric constant map from the s-SNOM image of a finite metallic disk, where the variation comes from the charge density induced by the em field.

The scattering-type near-field optical microscope (s-SNOM) has made great advances over the past decade by combining the well-developed atomic force microscope (AFM) techniques with a wide range of tunable and broadband light sources. By gathering the scattered light from an AFM tip [see Fig. 1(a)], s-SNOM effectively probes the near-field interactions between the nanometer-sized tip apex and the sample surface, providing a spatial resolution of 10 nm, far beyond the diffraction limit of traditional optics [1–3]. It has shown to be extremely useful in probing phase inhomogeneities in strongly correlated electron materials [2,4–8], polaritonic waves in two-dimensional materials [9–11], charge concentrations in semiconductor nanostructures [12–14], and molecular nano-fingerprints in organic and soft materials [15–17]. The central task of quantitatively understanding the near-field signals comes down to solving a nontrivial scattering problem, of which p-polarized light of frequency ω elastically scatters from a cone-shaped AFM tip, which oscillates vertically on the sample surface at the mechanical resonance frequency $\Omega \ll \omega$ of the cantilever. Approaches from simple models such as the point dipole [18] and r_p models [19] to elongated spheroid models [21,22,24] and state-of-the-art finite element calculations [20] have been applied to this problem. Because of the singularity at the tip, current approaches have not been able to consistently predict the near-field phase of the signal accurately (see Fig. 3 below). We find that the inverse extraction of the physical properties of the sample from the scattering data with current numerical approaches does not always produce unique results. It is also extremely time consuming to solve the problem without simplifying the approximation and this has limited the reliable real-time interpretation of the experimental data.

Here we overcame the difficulty of the singularity at the apex by using our recently developed technique [25–27] of representing the fields in basis functions containing integrable singularities at the tip obtained by conformal mapping between the cone and a round disk and successfully quantifying the elastic light scattering from a vibrating metallic tip. We found that with p-polarized light, the field-induced charge distribution consists of a bulk term along the body of the cone far away from the tip and localized terms at the tip apex and the base. The scattering at the fundamental frequency $\omega + \Omega$ comes from both the bulk and the localized charges. The near-field higher harmonic signals S_n at frequencies $\omega + n\Omega$ experimentally observed are dominated by contributions from the localized charge at the tip. In recent s-SNOM experiments at the optical to midinfrared range [2] (THz range) the fundamental is much larger than (comparable to) the higher harmonics respectively. Our calculation is in agreement with the empirical experiments where we found that the tip charge at THz frequencies is much larger than that at IR frequencies. To mimic the conical AFM tip, there has been work with different less singular tip geometries such as the spherical [18], the spheroidal [21–23], and the pear shaped [24]. These calculations implied different induced charge distributions. Our approach provides a more systematic way to calculate the charge distributions for different experimental conditions.

Our calculation is also orders of magnitude faster than current approaches and makes this study suitable for efficiently calculating the near-field signals and tip-sample interactions over a wide range of frequencies all the way from visible to terahertz with a fast and effective theoretical treatment. From the s-SNOM image of a finite metallic disk, we demonstrate the
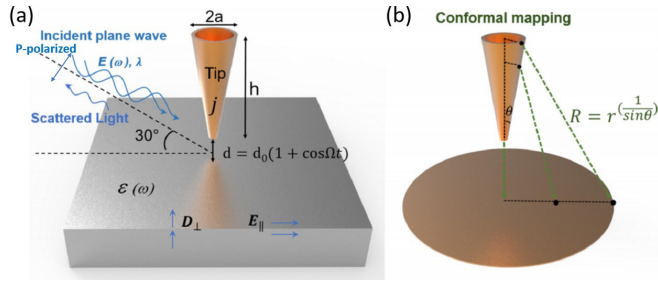
FIG. 1. (a) Schematic representation of the scattering near-field setup. The incident plane wave is p-polarized with the electric field $E(\omega)$. (b) Schematics of the conformal mapping of the cone-shaped tip to a round disk.

inverse extraction of a two-dimensional map which effectively quantifies the charge density of a finite metallic surface induced by an electromagnetic (em) field. We now describe our results in detail.

We are interested in the current flow in a finite metallic film wrapped in a cone shape caused by an external em wave. We assume that the film is thin enough that there is no current in the direction perpendicular to it. The current density $\mathbf{j}$ in the presence of an external electric field $\mathbf{E}_{\text{ext}}$ is governed by the equation

$$\rho\mathbf{j} - \mathbf{E}_{\text{em}} = \mathbf{E}_{\text{ext}}. \tag{1}$$

where ρ is the resistivity, $\mathbf{E}_{\text{em}}$ is the electromagnetic field generated by the current. We impose the boundary condition of no current flow perpendicular to the boundary of the film with a large boundary resistivity ρ_s which we take to approach infinity [25–27]. The total resistivity ρ is a sum of this boundary term and a metal resistivity ρ_0.

Because of the singularity at the tip, it is difficult to treat the problem. Here we represent the currents and the fields *not* in terms of finite elements on a mesh but in terms of a complete set of orthonormal basis functions with the integrable singularity of the system built in. This rigorous approach was shown to be very efficient [25–27]. For the simple case of an annulus of radii R_1, R_2, the basis functions are the well-known vector cylindrical functions [26,27] $\mathbf{M}_m$ $\mathbf{N}_m$ [28] of angular momentum m and with components X_r and X_Φ ($X = M, N$) in the radial and the angular directions. Here we are interested in a conical film of height h, base radius a with the cone angle $\theta = \tan^{-1} a/h$, thickness t, and a small flat tip of radius b [Fig. 1(a)]. This geometry is closest to the experimental setup among all the theoretical models. A point on the conical surface and a point inside the annulus are characterized by the cylindrical coordinates r and ϕ and R and Φ respectively. As illustrated in Fig. 1(b), these can be mapped into each other via a conformal harmonic map [29]

$$R = r^{1/\sin\theta}, \quad \Phi = \phi. $$

The Jacobian of the transformation is $J = R^{2\sin\theta - 2}$. We construct the basis function for this surface from the vector cylindrical harmonics of a circular annulus as

$$\mathbf{cX}(r) = \alpha\{X_r[\mathbf{R}(r)]\mathbf{e}_1 + X_\Phi\mathbf{e}_2,\} \tag{2}$$

where $X = M, N$, and $\alpha = 1/J^{1/2} = R/r$. The tangent vectors on the surface of the cone are in the cylindrical basis (r, ϕ, z): $\mathbf{e}_1 = 1/(1 + h^2)^{1/2}\mathbf{e}_r - h/(1 + h^2)^{1/2}\mathbf{e}_z$, $\mathbf{e}_2 = \mathbf{e}_\phi$ With this choice, these generalized vector cylindrical harmonics are orthonormal with the corresponding measure: $\int d^2r(\mathbf{cX_n})^* \cdot \mathbf{cY_m} = \int d^2R J|\alpha|^2\mathbf{X_n} \cdot \mathbf{Y_m} = \delta_{X,Y}$.

The electromagnetic field $\mathbf{E}_{\text{em}}$ can be represented as $\mathbf{E}_{\text{em}} = -\mathbf{Z^0 j}$ where the "impedance" matrix $\mathbf{Z^0}$ is just the representation of Green's function in this basis [25–27]. These integrals of Green's function were computed numerically with a subroutine that pays special attention to integrands with singularities. Just as in our previous studies, when the basis functions are orthonormal, the off-diagonal elements of the impedance matrix are much smaller than the diagonal elements. Furthermore the magnitude of the impedance increases rapidly. These greatly facilitate the convergence of the solution and provide for a much better understanding of the physics.

In this notation, the circuit equation becomes

$$\mathbf{Zj} = \mathbf{E}_{\text{ext}} + \mathbf{E}_s, \tag{3}$$

where $\mathbf{Z} = \mathbf{Z^0} + \mathbf{1}\rho_0$. The boundary electric field $\mathbf{E}_s$ is the product of the normal component of the current at the boundary j_s and $\rho_s(r)$, i.e. $\mathbf{E}_s = \mathbf{j}_s\rho_s$, $\rho_s(r) = 0$ when r is not at the boundaries. They behave like Lagrange multipliers. Their values are determined from the condition that the normal boundary currents become zero. Physically, as the external field is applied, the current is stopped at the boundary and charges of surface density σ_s are being accumulated. A boundary field is generated until it reaches a value to oppose further current arriving there.

In the experiment, there is an additional sample surface with dielectric constant ϵ underneath the cone. The em field induced charges of density n_c on the surface. In the presence of the plane at a distance $d = d_0(1 - \cos\Omega t) + d_m$ from the tip, there will be image charges of density $n_i(\mathbf{r} - 2d\mathbf{e}_z) = -\beta n_c(\mathbf{r})$ and $\beta = (\epsilon - 1)/(\epsilon + 1)$. Because d is much less than the wavelength, the method of image charges is a good approximation. The total em field now has additional contributions from the image charges, therefore the effective impedance $\mathbf{Z}$ is modified. We have calculated the additional image circuit parameters and included them in the circuit equations.

Because of the image charge, the tip surface field $E_{s2} = E_{sa} + E_{sb}$ is now a sum of a field E_{sa} from a surface charge of density σ_s at the tip and a field E_{sb} from the image charge density $-\beta\sigma_s$ at a distance $-d$ below the surface. From Gauss's law, $E_{sa} = \sigma_s/2\epsilon_0$ and $E_{sb} \approx -\beta\sigma_s/\epsilon_0 I(2d)$, where $I(x) = \langle E_{cz}\rangle$ is the z Coulomb electric field from the image charge density on the tip averaged over the tip. From these equations, we get

$$\sigma_s = 2\epsilon_0 E_{s2}/[1 - 2\beta I(2d)]. \tag{4}$$

We have calculated $I(x)$ numerically and tabulated it for a mesh of 4000 points in the region $0 < x/d_0 < 2$. Recent experiments have been carried out at IR frequency with $\lambda = 10$ μm, $h = 20$ μm, $a = 5$ μm, $b = 10$ nm, $d_0 = 60$ nm, $t = 20$ nm, and $d_m = 0.6$ nm and at THz frequency with λ centered at 300 μm, $h = 70$ μm, $a = 20$ μm, $b = 50$ nm, $d_0 = 150$ nm, and $d_m = 0.6$ nm [2,30]. In the latter case, the tip is solid; the effective thickness of the film is thus the skin depth ξ. For this case,
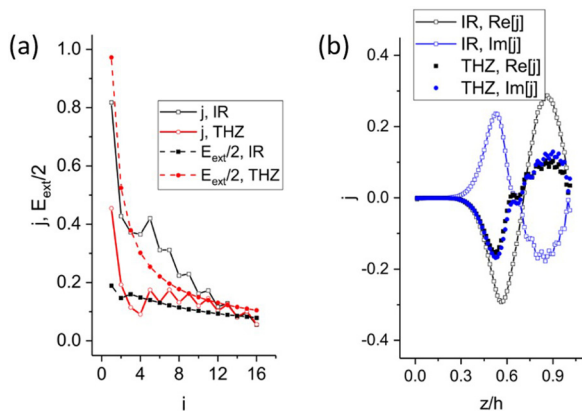
FIG. 2. Magnitude of the expansion coefficient for the bulk current density j^c (a) in terms of the normal mode wave vector index i in units of E_{ext}/ρ_u and (b) as a function of its normalized distance from the tip for parameters for two sets of experiments in the IR and THz regimes.

$t/a \approx 0.01$, whereas for the IR case, $t/a = 4 \times 10^{-3}$. We have carried out calculations for these parameters. The incoming field is at an angle of $60°$ with respect to the surface normal. This field is nearly uniform across the tip. The coupling is thus dominated by the $m = 0$ mode which we focus on.

We have calculated the circuit parameters $\mathbf{Z}$ for the $m = 0$ modes with the generalized vector cylindrical harmonics $cX_{m=0}(k_i r)$ for up to 16 wave vectors k_i. As usual, the magnitude of Z increases as k_i is increased. This makes the problem rapidly convergent in our approach. The expansion coefficients for the current density in the basis $c\mathbf{N}_0(k_i r)$ are shown in Fig. 2(a) where the nature of convergence of our expansion is illustrated. The current density $j = j^c j_u$ is in units of $j_u = E_{ext}/\rho_u$ where the resistivity unit is $\rho_u = Z_0 \omega a t/c$, Z_0 is the resistance of the vacuum. The IR experiments were carried out at a higher normalized wave vector and thus have more intermediate components. The magnitudes of the current densities as a function of the normalized position on the cone for both the IR and the THz experiments are shown in Fig. 2(b). The charge density contains a bulk contribution from currents inside the cone given by $n_c = -i\nabla \cdot j/\omega$. Because the current density is nearly zero around the tip at $z/h \approx 0$, its spatial derivative and hence this bulk charge density is only nonzero away from the tip at a distance much larger than d since $d/h \ll 1$. Thus this bulk charge will not contribute to near-field results. The total "bulk" charges in units of $Q_u = \epsilon_0 E_{ext} a^2$ for the THz case [$(-0.07+0.04i)$] and the IR case [$(-0.16+0.007i)$] are comparable in magnitude.

There are additional contributions to the charge from the surface charge densities localized at the tip (σ_{s2}) and the base (σ_{s1}). $\sigma_{si} = E_{si}\sigma_u$ where $\sigma_u = 2\epsilon_0 E_{ext}$. For the IR case, $E_{s1}/E_{ext} = 0.163 - 0.0168i, E_{s2}/E_{ext} = 4.374 + 6.23i$. For the THz case $E_{s1}/E_{ext} = 0.142 + 0.188i, E_{s2}/E_{ext} = -28.52 - 14.70i$. The magnitude of the surface charge at the tip in the THz case is five times larger than that for the IR experiments. This comes about because the wavelength of the external field is much closer to the size of the cone for the THz experiments, $E_{i,ext}$ is dominated by the component with $i = 1$, as is illustrated in Fig. 2.

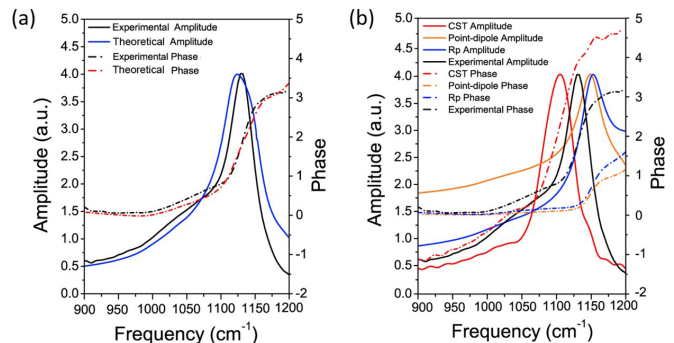FIG. 3. (a) Our theoretical and experimental results for the amplitude S_2 and the phase ϕ_2 of uniform SiO$_2$ as a function of frequency. (b) S_2 and ϕ_2 calculated with the r_p model, point-dipole model, and CST numerical solver, together with the experimental results.

We next look at the scattered field S_n at the modulated frequencies $\omega + n\Omega$ from the moving bulk and surface charges. The scattered fields at a distance r from the tip are proportional to the vector potential given by [31] $\mathbf{A}(r) = i\omega\mu_0 e^{ikr} \int d\mathbf{r}' \mathbf{j}(r')/r$. The *total* current density of the *vibrating* tip is a sum of a current induced by the incoming field and a current $j_d = n\partial_t d$ from the induced charge n and the vibration of the tip $\partial_t d$. n_c contains both bulk and boundary charge contributions. The bulk charges contribute mainly to the fundamental with $n = 1$. The contributions to the higher harmonics with $n > 1$ are dominated by near-field contributions when the tip is close to the surface and come mainly from the localized charge at the tip. The radiation electric field S_n is proportional to the Fourier transform at frequency $\omega + n\Omega$ of the contributions j_{dl} to j_d from the localized charges at the tip. From Eq. (4) we get

$$E \propto e^{i\omega t}(1 + \beta)\cos(\Omega t)/[1 - 2\beta I(d)]. \qquad (5)$$

As a test, we calculated the amplitude S_2 and its phase as a function of frequency using as input dielectric constants corresponding to a uniform surface of SiO$_2$. The experimental results together with our calculations are shown in the Fig. 3(a). The overall magnitude of the amplitudes and the baseline for the phase depend on the experimental geometry and thus are the two adjustable parameters. The agreement is very good. For comparison, results obtained with commonly used simple tip modeling as well as CST numerical simulation are plotted in Fig. 3(b), which do not show as good agreement with the experimental phase. This is due to the fact that finite-element simulations with sharp objects (singularities) lead to large mesh cell settings and therefore a lack of accuracy with reasonable calculation time.

The fundamental is comparable and much larger than the higher harmonics, respectively, in recent experiments carried out at the THz and the IR frequencies. The localized tip charge dominates the contribution to the higher harmonics and becomes much bigger for the THz experiments, providing an intuitive understanding of the origin of the near-field signals.

We close with an example of the inverse problem of extracting the physical properties from the measured [32] higher harmonics response for a gold disk of diameter approximately 1.3 μm and thickness ≈ 50 nm. We calculated a table of
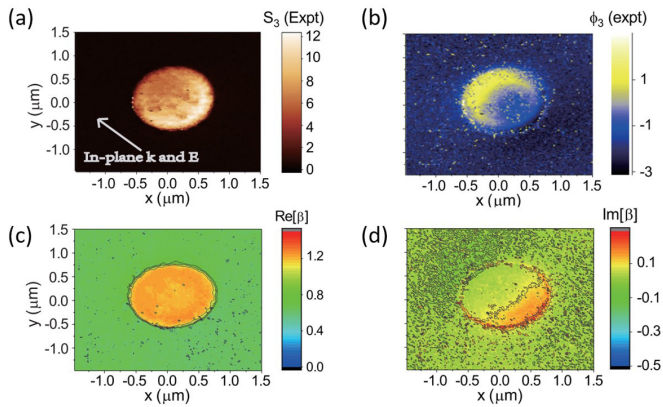
FIG. 4. Experimental (a) amplitude and (b) phase of the third harmonics as a function of position on the disk., and extracted values of (c) Re[β] and (d) Im[β], respectively.

S_3 and ϕ_3 as functions of $-0.1 < \text{Re}[\beta] < 1.4$, $-0.5 < \text{Im}[\beta] < 0.5$ from Eq. (5) for a mesh of 6400 grid points. This takes 2.7 s with a conventional Intel processor. For a pixel at position **r**, we go through the entries in our table and identify $\beta(\mathbf{r})$ as the one such that $|S_3(\beta(\mathbf{r})) - S_3^{\text{expt}}(\mathbf{r})| + |\phi_3(\beta(\mathbf{r})) - \phi_3^{\text{expt}}(\mathbf{r})|$ is minimized. This calculation takes 0.77 s for a data set of 128×128 pixels, making real-time data extraction possible.

Two-dimensional plots of β, S_3, and ϕ_3 are shown in Fig. 4. Even though the material exhibits the same intrinsic ϵ independent of position, there is a variation in the extracted β from the average value. This is due to charge densities on the disk induced by the incident em field. More precisely, β is determined from the condition that the change of the perpendicular component of the displacement field $D_\perp$ at the disk-air interface is equal to the surface charge density σ_{disk}: $\Delta D_\perp = \sigma_{\text{disk}}$. Our study of the em scattering on disks [26] suggests that there is an edge electric field and its associated charge at the perimeter of the disk. The variation of the physical quantities is indeed dominated by changes at the perimeter, in agreement with our expectation. An examination of the

quantitative values shows that the experimental amplitude and phase of the third harmonics are well reproduced. We found that $\text{Re}[\beta] \approx 1.2$ (0), $\text{Im}[\beta] \approx 0.07$ (0) inside (outside) the disk [33]. This technique may also be a new tool for mapping of the changes induced by external fields. The detailed analysis of this will be discussed in a separate paper.

In conclusion, we study the elastic scattering of an em wave by a conical metallic surface via representing the fields on the surface in generalized vector cylindrical harmonics containing the integrable singularities at the tip. We applied our calculation to s-SNOM and found good agreement with experimental results from a vibrating metallic tip over a uniform sample. We found the field-induced charge distribution consists of a bulk term along the body of the cone and localized terms at the tip apex and the base. The bulk charge is far away from the tip and contributes little to the near-field higher harmonics in the scattered field. The localized boundary charges at the tip apex contribute to the near-field signal and correspond to the charge accumulation effects previously discussed in pn junctions and on the surface of capacitor plates in ac experiments [34–36]. In these treatments, the additional physics of the diffusion of the electrons are included and a finite width in the localized charge distribution of the order of the screening length is found. This localized boundary charge provides insight into the physics of the scattering problem, which can be related to the distinct S_1/S_2 ratio found in recent experiments at IR and THz frequencies. In addition, we also demonstrate the application of our technique by extracting a two-dimensional effective dielectric constant map of a finite plasmonic metallic disk from experimental data, which is nonuniform due to the induced charge density distribution under the illumination of an em field. Our calculations of the scattering signal and the back-extraction process are more realistic and much faster compared to the prevailing analytical and numerical approaches. Future studies will include the calculation of near-field scattering signals of nonuniform samples.

[1] L. Novotny, Prog. Opt. **50**, 137 (2008).

[2] M. Liu, A. J. Sternbach, and D. N. Basov, Rep. Prog. Phys. **80**, 14501 (2017).

[3] See Supplemental Material at http://link.aps.org/supplemental/10.1103/PhysRevB.97.081406 for background information and details.

[4] M. M. Qazilbash, M. Brehm, B.-G. Chae, P.-C. Ho, G. O. Andreev, B.-J. Kim, S. J. Yun, A. V. Balatsky, M. B. Maple, F. Keilmann, H.-T. Kim, and D. N. Basov, Science **318**, 1750 (2007).

[5] S. A. Dönges, O. Khatib, B. T. O'Callahan, J. M. Atkin, J. H. Park, D. Cobden, and M. B. Raschke, Nano Lett. **16**, 3029 (2016).

[6] M. A. Huber, M. Plankl, M. Eisele, R. E. Marvel, F. Sandner, T. Korn, C. Schüller, R. F. Haglund, R. Huber, and T. L. Cocker, Nano Lett. **16**, 1421 (2016).

[7] M. K. Liu, M. Wagner, E. Abreu, S. Kittiwatanakul, A. McLeod, Z. Fei, M. Goldflam, S. Dai, M. M. Fogler, J. Lu, S. A. Wolf,

R. D. Averitt, and D. N. Basov, Phys. Rev. Lett. **111**, 096602 (2013).

[8] A. S. McLeod, E. van Heumen, J. G. Ramirez, S. Wang, T. Saerbeck, S. Guenon, M. Goldflam, L. Anderegg, P. Kelly, A. Mueller, M. K. Liu, I. K. Schuller, and D. N. Basov, Nat. Phys. **13**, 80 (2017).

[9] Z. Fei, A. S. Rodin, G. O. Andreev, W. Bao, A. S. McLeod, M. Wagner, L. M. Zhang, Z. Zhao, M. Thiemens, G. Dominguez, M. M. Fogler, A. H. Castro Neto, C. N. Lau, F. Keilmann, and D. N. Basov, Nature **487**, 82 (2012).

[10] J. Chen, M. Badioli, P. Alonso-Gonzlez, S. Thongrattanasiri, F. Huth, J. Osmond, M. Spasenovi, A. Centeno, A. Pesquera, P. Godignon, A. Zurutuza Elorza, N. Camara, F. J. G. de Abajo, R. Hillenbrand, and F. H. L. Koppens, Nature **487**, 77 (2012).

[11] S. Dai, Q. Ma, M. K. Liu, T. Andersen, Z. Fei, M. D. Goldflam, M. Wagner, K. Watanabe, T. Taniguchi, M. Thiemens, F.

Keilmann, G. C. a. M. Janssen, S.-E. Zhu, P. Jarillo-Herrero, M. M. Fogler, and D. N. Basov, Nat. Nanotechnol. **10**, 682 (2015).

[12] F. Buersgens, R. Kersting, and H. T. Chen, Appl. Phys. Lett. **88**, 112115 (2006).

[13] K. Moon, H. Park, J. Kim, Y. Do, S. Lee, G. Lee, H. Kang, and H. Han, Nano Lett. **15**, 549 (2015).

[14] A. J. Huber, F. Keilmann, J. Wittborn, J. Aizpurua, and R. Hillenbrand, Nano Lett. **8**, 3766 (2008).

[15] H. A. Bechtel, E. A. Muller, R. L. Olmon, M. C. Martin, and M. B. Raschke, Proc. Natl. Acad. Sci. USA **111**, 7191 (2014).

[16] I. Amenabar, S. Poly, M. Goikoetxea, W. Nuansing, P. Lasch, and R. Hillenbrand, Nat. Commun. **8**, 14402 (2017).

[17] N. Qin, S. Zhang, J. Jiang, S. G. Corder, Z. Qian, Z. Zhou, W. Lee, K. Liu, X. Wang, X. Li, Z. Shi, Y. Mao, H. A. Bechtel, M. C. Martin, X. Xia, B. Marelli, D. L. Kaplan, F. G. Omenetto, M. Liu, and T. H. Tao, Nat. Commun. **7**, 13079 (2016).

[18] F. Keilmann and R. Hillenbrand, Philos. Trans. R. Soc. London A **362**, 787 (2004).

[19] S. Dai, Z. Fei, Q. Ma, A. S. Rodin, M. Wagner, A. S. McLeod, M. K. Liu, W. Gannett, W. Regan, K. Watanabe, T. Taniguchi, M. Thiemens, G. Dominguez, A. H. C. Neto, A. Zettl, F. Keilmann, P. Jarillo-Herrero, M. M. Fogler, and D. N. Basov, Science **343**, 1125 (2014).

[20] Numerical calculations with the commercial software COMSOL was reported by many authors but we could not find any published result for the phase. We have carried out calculations with a comparable commercial software CST STUDIO [X. Chen, C. F. B. Lo, W. Zheng, H. Hu, Q. Dai, and M. Liu, Appl. Phys. Lett. **111**, 223110 (2017)], and the amplitude and the phase is reported below.

[21] A. Cvitkovic, N. Ocelic, and R. Hillenbrand, Opt. Express **15**, 8550 (2007).

[22] A. S. McLeod, P. Kelly, M. D. Goldflam, Z. Gainsforth, A. J. Westphal, G. Dominguez, M. H. Thiemens, M. M. Fogler, and D. N. Basov, Phys. Rev. B **90**, 085136 (2014).

[23] B. Hauer, A. P. Engelhardt, and T. Taubner, Opt. Express **20**, 13173 (2012).

[24] B.-Y. Jiang, L. M. Zhang, A. H. Castro Neto, D. N. Basov, and M. M. Fogler, J. Appl. Phys. **119**, 054305 (2016).

[25] S. T. Chui and L. Zhou, *Electromagnetic Behaviour of Metallic Wire Structures* (Springer, New York, 2013).

[26] S. T. Chui, J. J. Du, and S. T. Yau, Phys. Rev. E **90**, 053202 (2014).

[27] S. T. Chui, S. Wang, and C. T. Chan, Phys. Rev. E **93**, 033302 (2016).

[28] See "Basis function" in the Supplemental Material [3].

[29] J. H. Lambert, *Notes and Comments on the Composition of Terrestrial and Celestial Maps* (ESRI Press, 1772) (Translated and Introduced by W. R. Tobler, 1972).

[30] P. Alonso-González, A. Y. Nikitin, Y. Gao, A. Woessner, M. B. Lundeberg, A. Principi, N. Forcellini, W. Yan, S. Vélez, A. J. Huber, K. Watanabe, T. Taniguchi, F. Casanova, L. E. Hueso, M. Polini, J. Hone, F. H. L. Koppens, and R. Hillenbrand, Nat. Nanotechnol. **12**, 31 (2016).

[31] J. D. Jackson, *Classical Electrodynamics* (Wiley, New York, 1998), Eq. (9.13).

[32] X. Chen and M. Liu (unpublished).

[33] See the last section in the Supplemental Material [3].

[34] C. Kittel, *Introduction to Solid State Physics* (Wiley, New York, 2004), Chap. 8.

[35] S. T. Chui and L. Hu, Appl. Phys. Lett. **80**, 273 (2002).

[36] A. F. Hebard, S. A. Ajuria, and R. H. Eick, Appl. Phys. Lett. **51**, 1349 (1987).